Electronic Supplementary Material (ESI) for Journal of Materials Chemistry A.

Supplementary Information

Vapor induced phase separation towards anion-/near-infrared-responsive pore channels for switchable anti-fouling membranes

Ran Wei[a], Jiabei Guo[a], Lunqiang Jin[a], Chao He[a], Yi Xie[a], Xiang Zhang[ab]*, Weifeng Zhao[a] and Changsheng Zhao[ac]*

[a] College of Polymer Science and Engineering, State Key Laboratory of Polymer Materials Engineering, College of Chemical Engineering, Sichuan University, Chengdu 610065, People’s Republic of China.

[b] Institute for Chemical Technology and Polymer Chemistry, Karlsruhe Institute of Technology, Karlsruhe 76128, Germany.

[c] National Engineering Research Centre for Biomaterials, Sichuan University, Chengdu 610064, People's Republic of China.

* Corresponding author.

Email: zhangxiangscu2011@163.com (Xiang Zhang);
zhaochsh70@163.com, zhaochsh70@scu.edu.cn (Changsheng Zhao)

Tel: 86 28 85400453; Fax: 86 28 85405402

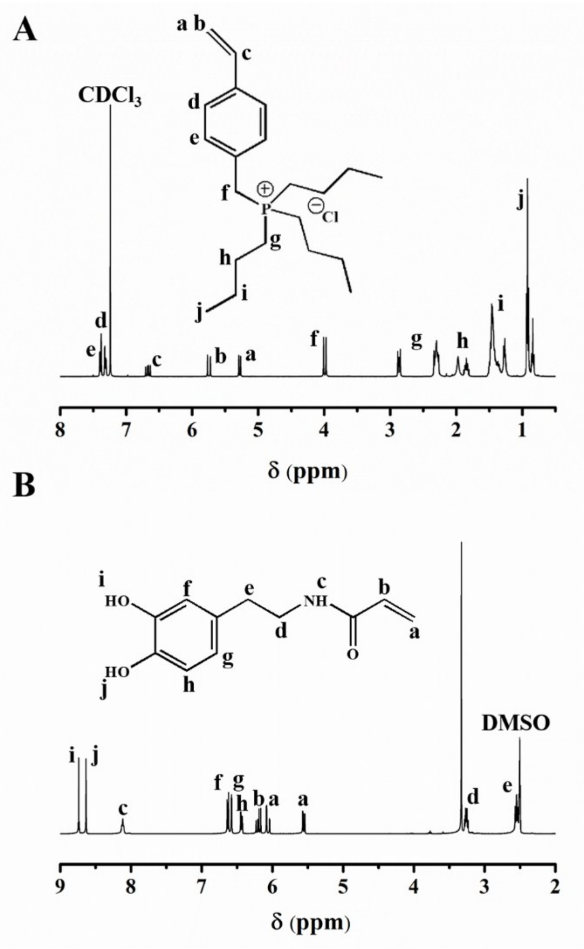

Figure S1. (A) ^{1}HNMR spectrum of TVBP-Cl in $CDCl_3$. (B) ^{1}HNMR spectrum of in DMSO.

^{1}HNMR (400 MHz, $CDCl_3$): δ 6.67 (dd, J = 17.6, 10.9 Hz, 0H), 5.75 (d, J = 17.6 Hz, 0H), 5.28 (d, J = 10.9 Hz, 0H), 3.99 (d, J = 15.1 Hz, 0H), 2.87 (dd, J = 9.8, 6.5 Hz, 0H), 2.48 – 2.15 (m, 0H), 1.91 (d, J = 50.8 Hz, 0H), 1.67 – 1.06 (m, 1H), 0.90 (dd, J = 23.0, 15.9 Hz, 1H).

^{1}H NMR (400 MHz, DMSO-*d_6*): δ 8.68 (d, J = 41.1 Hz, 1H), 8.11 (t, J = 5.4 Hz, 1H), 6.52 (ddd, J = 15.6, 9.9, 4.9 Hz, 1H), 6.13 (ddd, J = 19.4, 17.1, 6.2 Hz, 1H), 5.56 (dd, J = 10.0, 2.3 Hz, 1H), 3.62 – 3.06 (m, 2H), 2.71 – 2.34 (m, 2H).

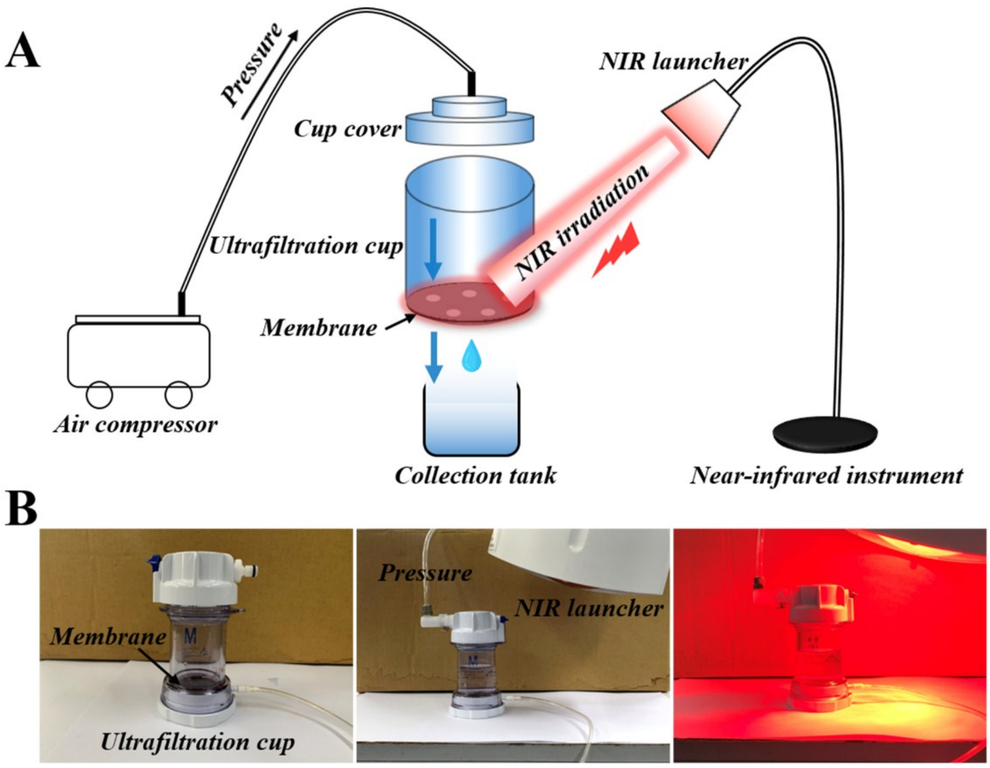

Figure S2. (A) Schematic illustration of the filtration experiment under NIR-light. (B) The digital photographs of the ultrafiltration cup and the filtration experiment under NIR-light.

Water fluxes of the membranes were obtained via a transparent dead-end ultrafiltration cup (Millipore, UFSC5001, USA), the effective area was 15.2 cm^2 and the filtration pressure was 0.1 MPa. The NIR irradiation were provided by the near-infrared therapeutic instrument (Lifowave-9350B, China). For the filtration experiment under NIR-light, the membranes were irradiated with NIR (50 mW/cm^2) for 10 min to get steady flux, then water fluxes of the membranes under NIR light were measured for another 20 min, as shown in **Fig. S2**.

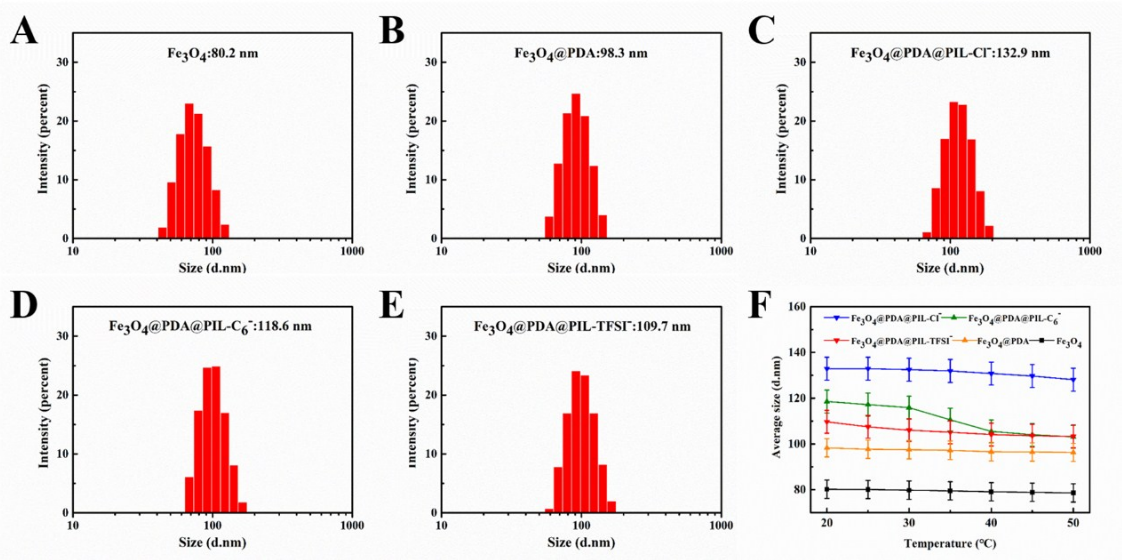

Figure S3. The DLS data of the (A) Fe$_3$O$_4$, (B) Fe$_3$O$_4$@PDA, (C) Fe$_3$O$_4$@PDA@PIL-Cl$^-$, (D) Fe$_3$O$_4$@PDA@PIL-C$_6^-$ and (E) Fe$_3$O$_4$@PDA@PIL-TFSI$^-$. (F) The DLS data of the Fe$_3$O$_4$, Fe$_3$O$_4$@PDA, Fe$_3$O$_4$@PDA@PIL-Cl$^-$, Fe$_3$O$_4$@PDA@PIL-C$_6^-$ and Fe$_3$O$_4$@PDA@PIL-TFSI$^-$ with different temperature.

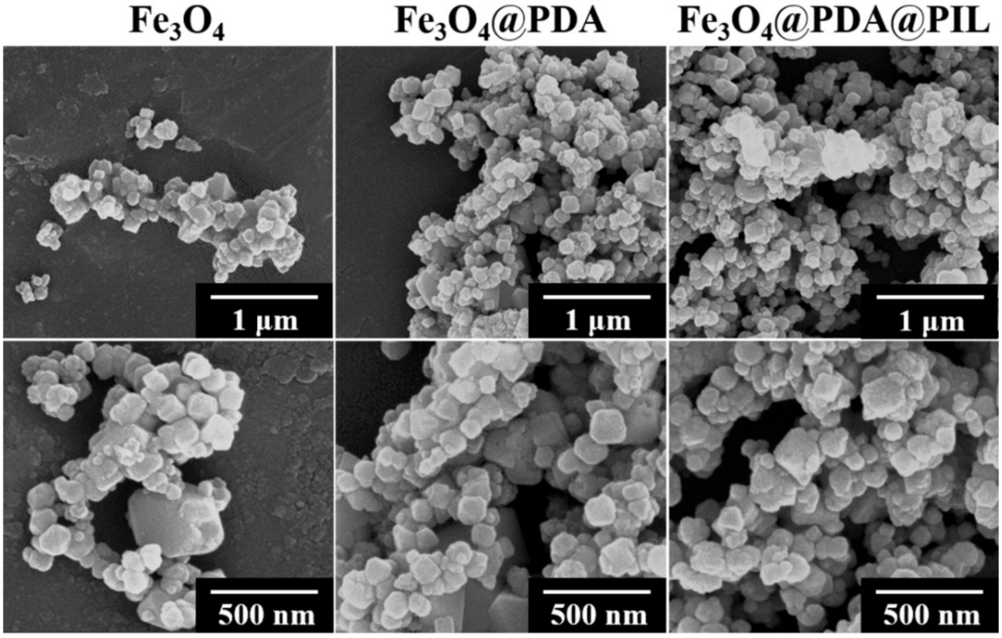

Figure S4. The SEM images of the Fe_3O_4, Fe_3O_4@PDA and Fe_3O_4@PDA@PIL.

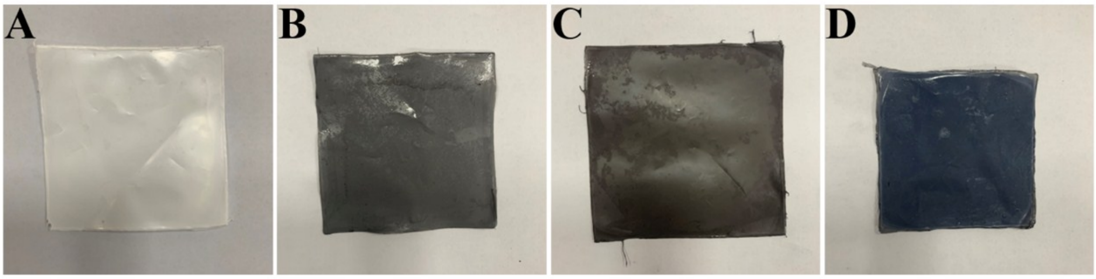

Figure S5. The digital photographs of the prepared membranes (A) M-PES via VIPS, (B) M-Fe_3O_4 via VIPS, (C) M-PIL via VIPS and (D) M-PIL via LIPS.

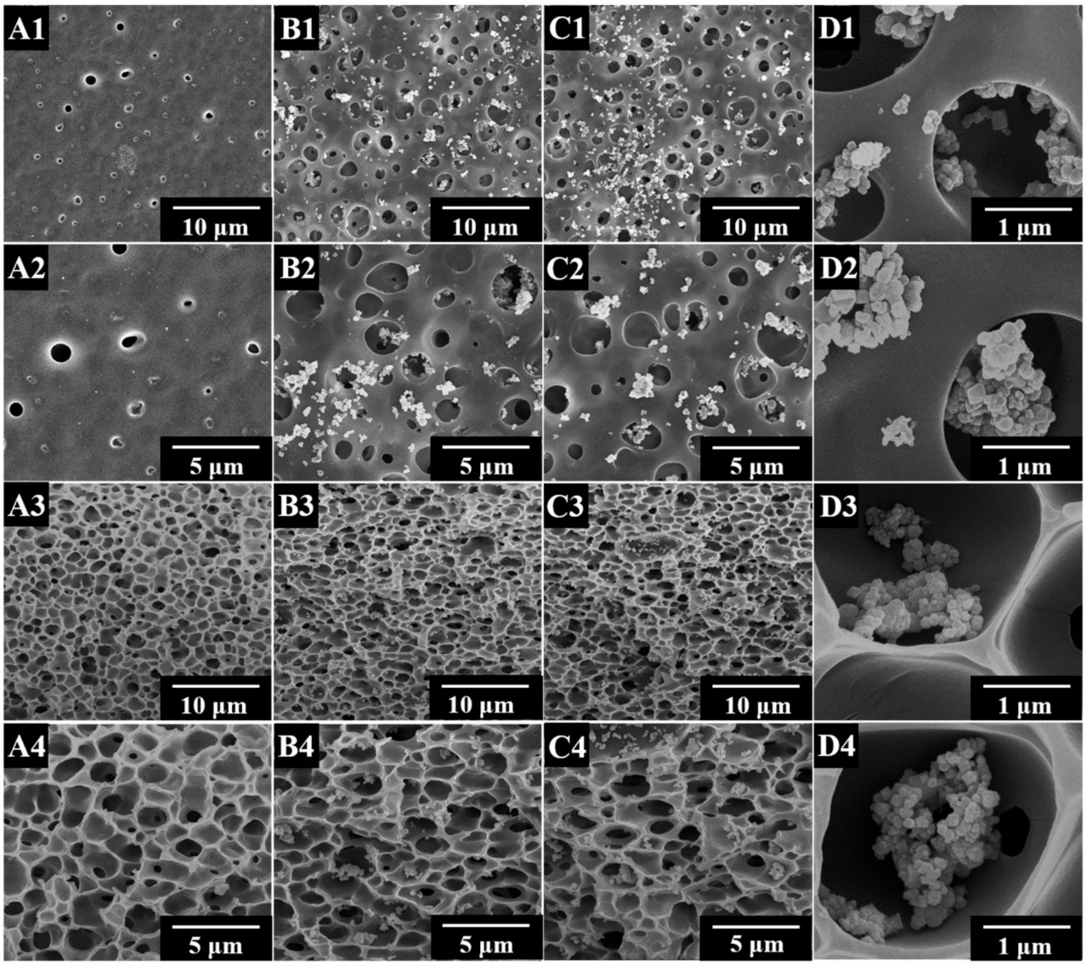

Figure S6. The surface and cross-section SEM images of the membranes via VIPS. (A1)-(A4) M-PES. (B1)-(B4) M-Fe_3O_4. (C1)-(C4) M-PIL. (D1)-(D4) The magnified SEM images of M-PIL.

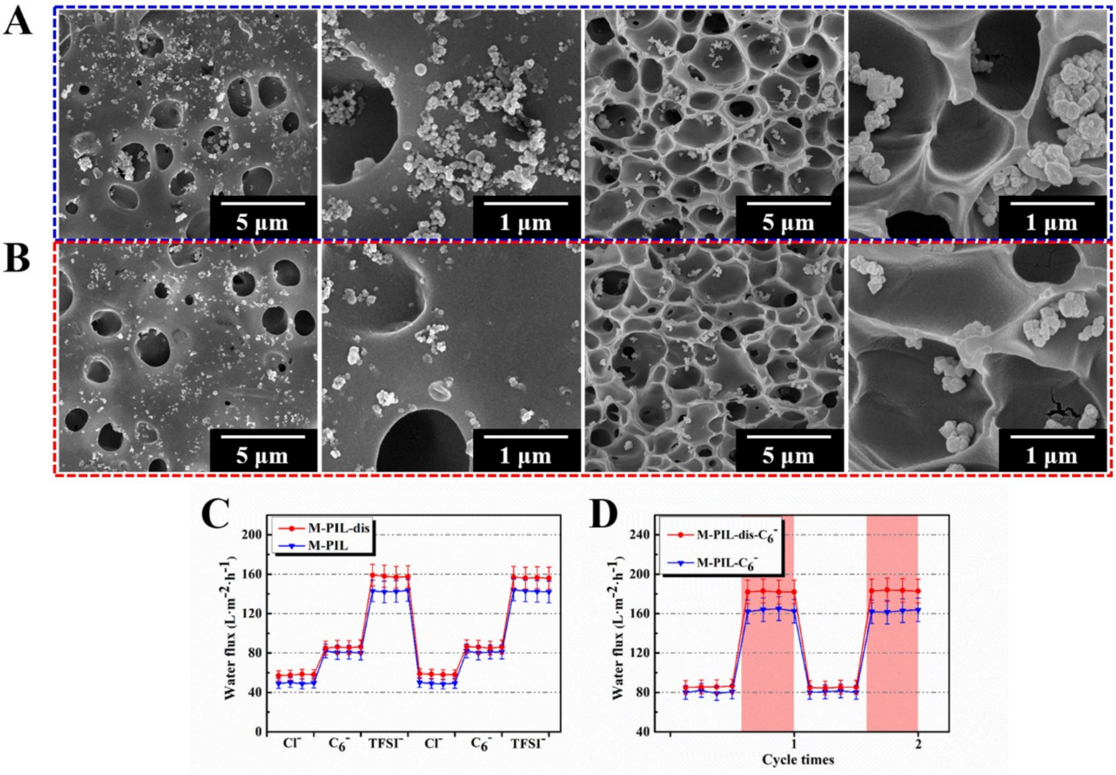

Figure S7. (A) The surface and cross-section SEM images of M-PIL. (B) The surface and cross-section SEM images of M-PIL-dis. (C) The anion-responsive behaviors of the M-PIL-C_6^- and M-PIL-dis-C_6^-. (D) The NIR-responsive behaviors of the M-PIL and M-PIL-dis.

In **Fig. S7A**, macro-aggregations of the nanoparticles were observed in the surface and cross-section SEM images of M-PIL. To distribute the nanoparticles more uniformly, the Fe_3O_4@PDA@PIL nanoparticles were exchanged to $TFSI^-$ (the hydrophobic counteranion) in advance, then the membranes were fabricated and the SEM images were shown in **Fig. S7B**. In **Fig. S7B**, although the aggregation of the nanoparticles still existed, the amounts of the aggregations decreased. Therefore, it was possible to distribute the nanoparticles in the whole bulk more uniformly by exchanging the counteranions to hydrophobic ones in advance. Before and after the modification, the water fluxes of the membranes with different counteranions and NIR irradiation were tested, and the results were shown in **Fig. S7C** and **D**. The water fluxes increased slightly after the modifications, the anion-responsive and NIR-responsive behaviors of the membranes were unchanged after the modifications, which indicated that the distribution of the nanoparticles in membranes were insignificant to the separation properties of the membranes.

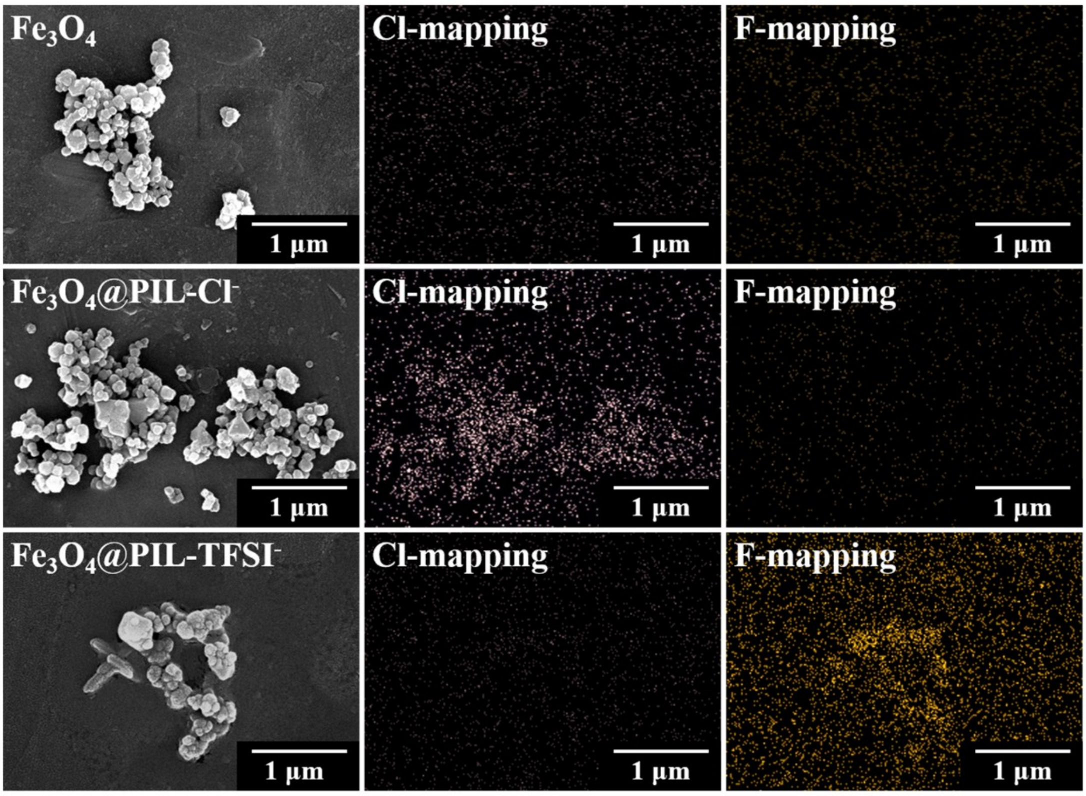

Figure S8. The SEM images of the Fe_3O_4, Fe_3O_4@PDA@PIL-Cl^- and Fe_3O_4@PDA@PIL-$TFSI^-$.(left) The Cl distribution on the surface of the nanoparticles analyzed by EDS-mapping.(middle) The F distribution on the surface of the nanoparticles analyzed by EDS-mapping.(right)

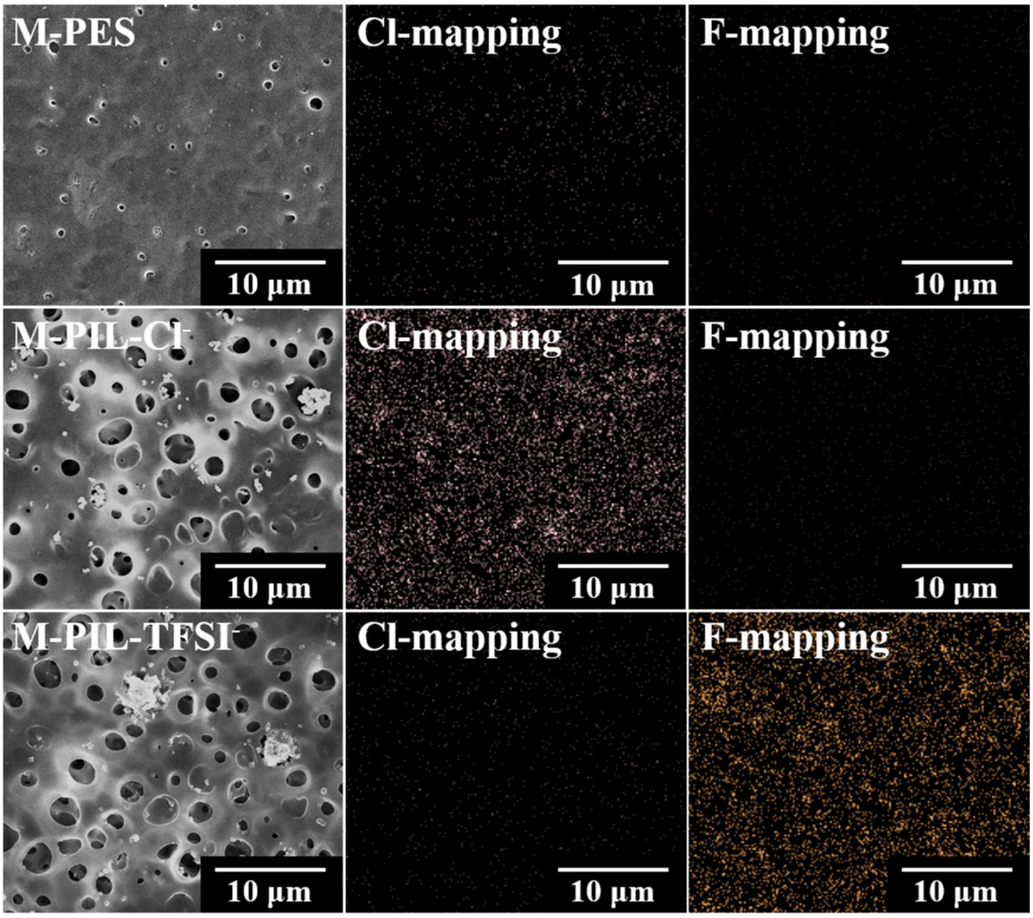

Figure S9. The surface SEM images of the M-PES, M-PIL-Cl^- and M-PIL-$TFSI^-$.(left) The Cl distribution on the surface of the membranes analyzed by EDS-mapping.(middle) The F distribution on the surface of the membranes analyzed by EDS-mapping.(right)

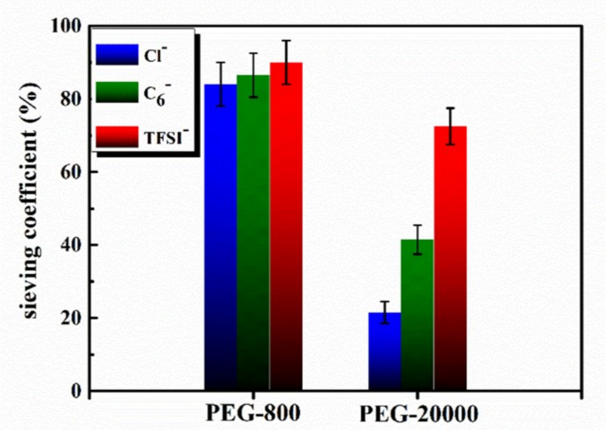

Figure S10. The sieving property of the M-PIL for PEG-800 and PEG-20000 with different counteranions.

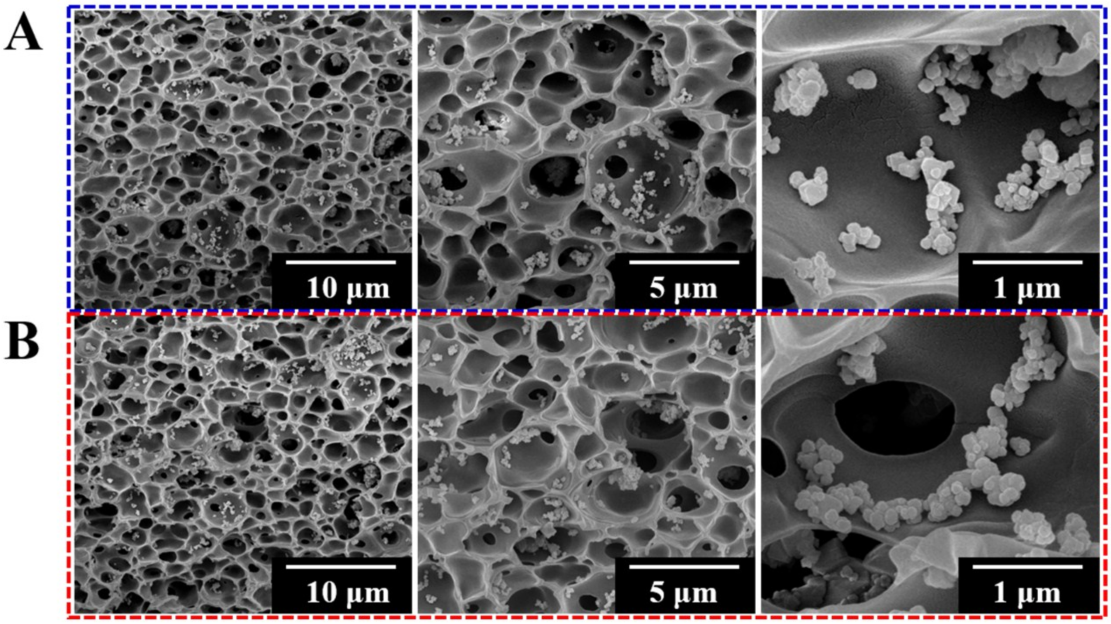

Figure S11. (A) The cross-section SEM images of the M-PIL-Cl^-. (B) The cross-section SEM images of the M-PIL-$TFSI^-$.

To investigate the nanoparticles aggregation and expansion with different counteranions, the M-PIL with Cl^- and $TFSI^-$ were prepared and the cross-section SEM images were provided in **Fig. S11**. In **Fig. S11A**, the nanoparticles aggregations could be observed on the pore channels of the M-PIL-Cl^-. The nanoparticles were immobilized on the pore channels and the channels were interconnected. The aggregation and expansion of the nanoparticles were different, and the distribution of the nanoparticles were not uniformed in the pore channels with different pore size. In **Fig. S11B**, the counteranion was changed to hydrophobic one ($TFSI^-$), the aggregation and distribution of the nanoparticles showed no difference with that for M-PIL-Cl^-. The result of the SEM demonstrated that in the membranes, the aggregation and distribution of the nanoparticles have not changed after exchanging the counteranions from hydrophilic to hydrophobic ones. Therefore, the pore sizes (water fluxes) were mainly determined by the sizes of the PIL nanoparticles.

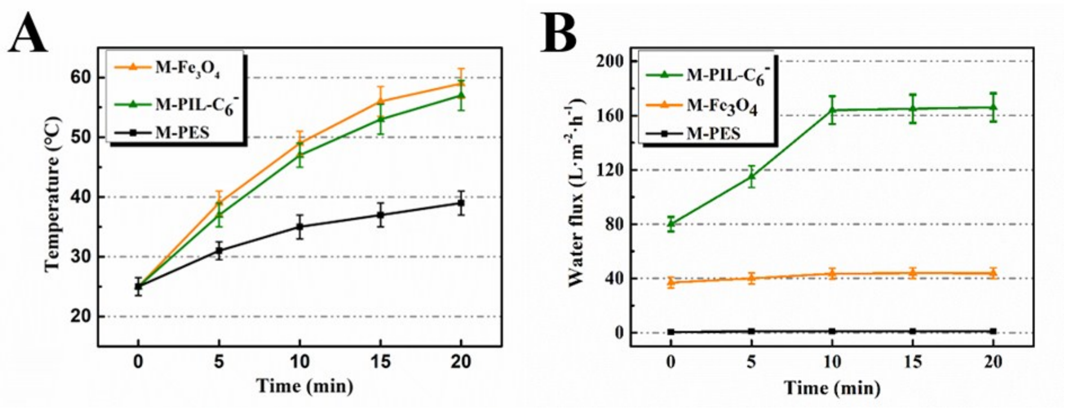

Figure S12. (A) The temperature of the membranes with different NIR irradiation time. (B) The water fluxes of the membranes with different NIR irradiation time.

To better investigate the temperature and water flux change under NIR-light (808 nm, 50 mW/cm^2, 0-5 min) during the filtration experiment, the temperature was also measured by a thermal imager (FLUKE TiS50), and the results were shown in **Fig. S12A**. The temperature of the M-PES increased from 25 ^{o}C to 39 ^{o}C after irradiation for 20 min, the temperature of the M-Fe$_3$O$_4$ and M-PIL-C$_6^-$ reached to 59 ^{o}C and 55 ^{o}C after irradiation for 20 min, respectively. During the filtration test, the temperature increase was slower because the thermal energy was dissipated by the flowing water. Then the water fluxes of the membranes were also obtained, as shown in **Fig. S12B**. For the M-PES and M-Fe$_3$O$_4$, the water fluxes showed small boost after irradiation with NIR. For the M-PIL-C$_6^-$, the water flux increased from 80 L/m$^{-2}\cdot$h^{-1} to 165 L/m$^{-2}\cdot$h^{-1} under the irradiation of NIR for the first 10 min, then the water flux barely increased afterwards. Therefore, the water flux of the M-PIL-C$_6^-$ showed rapid increase under the NIR irradiation, and the steady filtration could be reached after 10 min.

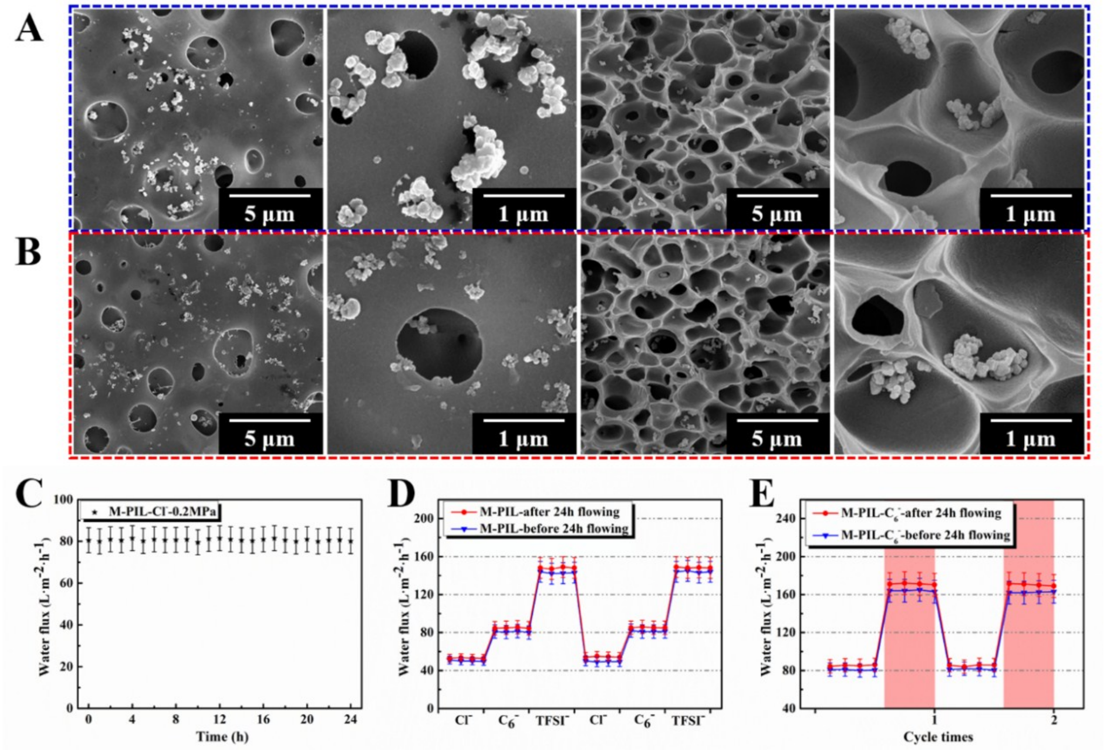

Figure S13. (A) The surface and cross-section SEM images of the M-PIL-before 24h flowing. (B) The surface and cross-section SEM images of the M-PIL-after 24h flowing. (C) Under 0.2 MPa, the water fluxes of the M-PIL at different time. (D) The anion-responsive behaviors of the M-PIL-before 24h flowing and M-PIL-after 24h flowing. (E) The NIR-responsive behaviors of the M-PIL-before 24h flowing and M-PIL-after 24h flowing.

The water fluxes of the M-PIL-Cl^- were tested for 24 h under 0.2 MPa, the SEM images of the membranes before and after the test were shown in **Fig. S13A** and **B**. In **Fig. S13A**, the nanoparticles showed aggregation and distribution on the membrane surface and inside the pores. After tested for 24 h, the SEM results in **Fig. S13B** indicated that the aggregation and distribution of the nanoparticles slightly decreased on the membranes surface, and unchanged inside the pores. During the test, the water fluxes stabilized around 80 $L/m^{-2}\cdot h^{-1}$, as shown in **Fig. S13C**. Before and after the flowing test, the water fluxes of the membranes with different counteranions and NIR irradiation were tested, and the results were shown in **Fig. S13D** and **E**. The water fluxes increased slightly after the flowing test, the anion-responsive and NIR-responsive behaviors of the membranes unchanged after the flowing test, which indicated that the bonding stability of the nanoparticles were robust enough to guarantee the fluxes stability via long-term vigorous flowing wash.

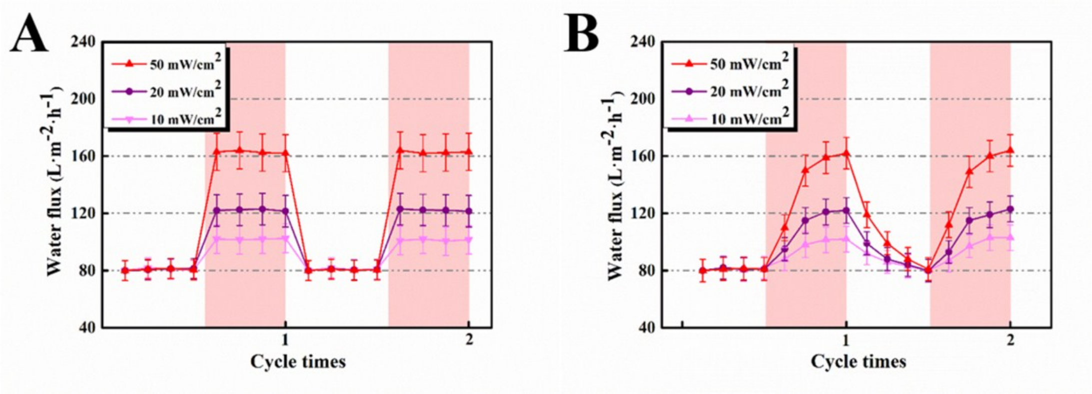

Figure S14. (A) The water fluxes of the M-PIL-C_6^- with different NIR power densities.(the fluxes were obtained when the fluxes reached the equilibrium under NIR irradiation) (B) The water fluxes of the M-PIL-C_6^- with different NIR power densities.(the fluxes under NIR irradiation were obtained right after the NIR turning on)